Co-published by
Institute of Fluid-Flow Machinery
Polish Academy of Sciences
Committee on Thermodynamics and Combustion
Polish Academy of Sciences

http://www.imp.gda.pl/archives-of-thermodynamics/

ARCHIVES OF THERMODYNAMICS

Numerical Investigation of a Two-Stage Ejector Based on a Constant Rate of Momentum Change: Performance Analysis and Optimisation

Arvind Kumar[a], Surendra Kumar Yadav[a*], Virendra Kumar[b]

[a]Department of Mechanical Engineeringirst, K.R. Mangalam University, Gurugram 122001, India
[b]Department of Mechanical Engineering, Madan Mohan Malviya University, Gorakhpur 273016, India
*Corresponding author email: s.k.yadav86@gmail.com

Received: 01.04.2025; revised: 17.07.2025; accepted: 19.07.2025

Abstract

A two-stage ejector based on a constant rate of momentum change is a geometrical arrangement of a single-stage ejector to further improve its performance, utilising water vapour as a working fluid for both primary and secondary flows. Creating an additional secondary inlet in the single-stage ejector helps to further entrain the secondary mass flow, resulting in a better entrainment ratio. The present study utilises the constant rate of momentum change, and a 1D gas dynamic approach to compute the geometrical profile and flow parameters using MATLAB. The numerical software ANSYS Fluent 18.0 is utilised to analyse the two-stage ejector geometry. The global performance ejector entrainment was computed at on and off design conditions. The results show that the two-stage ejector entrainment ratio is significantly higher than that of the previously studied single-stage ejector. The entrainment ratio of the two-stage ejector increases to reach the on-design value of operating conditions, and then starts decreasing.

Keywords: Constant rate of momentum change; Ejector; Two-stage; CFD.

Vol. 46(2025), No. 4, 7–17; doi: 10.24425/ather.2025.156597

Cite this manuscript as: Kumar, A., Yadav, S. K., & Kumar, V. (2025). Numerical Investigation of a Two-Stage Ejector Based on a Constant Rate of Momentum Change: Performance Analysis and Optimisation. *Archives of Thermodynamics*, 46(4), 7−17.

1. Introduction

An ejector is a device that utilises the Venturi effect to create a vacuum and entrain gas or vapour from a desired vessel or system. In this study, the two-stage ejector (TSE) operates with water vapour as a working fluid for both primary and secondary flows, leveraging the constant rate of momentum change (CRMC) approach to enhance the ejector performance. It works similarly to a vacuum pump but without any moving parts. In the early 19th century (1942), the ejector model was developed by Keenan J. H. and Neumann E. P. These ejectors are built on constant area and pressure mixing (CAM and CPM) approaches. Several efforts have been made to optimise the ejector parameters, viz. nozzle parameters [1], mixing section geometrical parameters [2], diffuser geometrical parameters [3] and ejector operating parameters [4]. Even after all efforts made to improve both CAM and CPM single stage ejectors, their performance is limited. It is found that the CPM ejector exhibits a better performance than that of the CAM ejectors [5]. A novel method for a comprehensive analysis of geometric properties that can be used to alter the mass flow ratio and the hydrogen mass flow was introduced. Additionally, the dynamic behaviour of the fuel cell system's ejector was investigated in [6]. According to energy, exergy, and economic considerations, the goal of the recent study [7] was to thoroughly examine the performance of a solar ejector cooling system. It was meant to provide a complete view of the solar cooling system performance under typical operational circumstances.

Nomenclature

L – length, m
M – Mach number
$\dot{m}$ – mass flow rate, kg/s
T – temperature, K
P_d – discharge pressure, Pa
P_s – suction pressure, Pa
u – velocity, m/s

Greek symbols

ρ – density, kg/m^3
φ – entrainment ratio

Subscripts

e – exit flow
I, J – space component
m – mixing
n – nozzle
o – stagnation condition
p – primary fluid flow
s – secondary fluid flow
$s1$ – secondary fluid flow (Stage I)
$s2$ – secondary fluid flow (Stage II)

Abbreviations and Acronyms

CAM – constant area mixing
CFD – computational fluid dynamics
CPM – constant pressure mixing
CRMC – constant rate of momentum change
RANS – Reynolds-averaged Navier-Stokes
SSE – single-stage ejector
TEWI – total equivalent warming impact
TSE – two-stage ejector

Kanbur et al. (2025) [8] used a coupled CFD and thermodynamic model to define outlet boundary conditions through multiphase CFD simulations. The study claims that this framework reduces reliance on experimental data. A comprehensive assessment of energy, exergy, and economic factors conducted by Ogaili et al. [9] highlights an integrated solar-thermal power system, which leads to more sustainable and cost-effective energy solutions. The single-compression multi-temperature ejector refrigeration sequence architecture is proposed by Fabris et al. [10] for last-mile deliveries of multi-temperature goods in urban environments. The design of ejectors helps effectively to reduce the overall carbon footprint associated with road transport refrigeration systems. These results have significant implications for the design and deployment of hybrid refrigeration systems that seek to reduce their ecological influence while upholding operational flexibility [11].

The current investigation involved an experimental analysis of a gas ejector with a spindle calculated for use with propane (R290) as a working fluid. The performance of the ejector was assessed using conventional literature notation, the critical temperature and entrainment ratio, which are the supreme important factors for adjusting cooling capability in ejector-based refrigeration methods [12]. In order to optimise the ejector performance, the surrogate model developed in [13] uses a multi-objective evolutionary approach to increase entrainment and compression ratios while reducing entropy output. The stagnation temperature ratio is found to be one of the main factors that enhances mixing layer growth and ejector performance. The optimised ejector shows a roughly 25% boost in efficiency over a non-optimised one. The study [14] looks at how well four cutting-edge cascaded refrigeration systems work to cool at lower temperatures while consuming less energy. In a flash binary geothermal cycle, the study [15] offers a new method to increase the efficiency of a geothermal-based power plant by substituting an ejector for conventional expansion valves.

A two-stage ejector (TSE) is a type of ejector system that involves two stages of compression or fluid entrainment to achieve the desired pressure or flow rate (refer to Fig. 1). Ejectors, also known as jet pumps, are devices that use the principle of fluid dynamics to transfer or compress fluids. They operate by entraining a secondary fluid or gas using a high-speed primary fluid, typically at a nozzle or diffuser, creating a low-pressure section that draws in the secondary fluid.

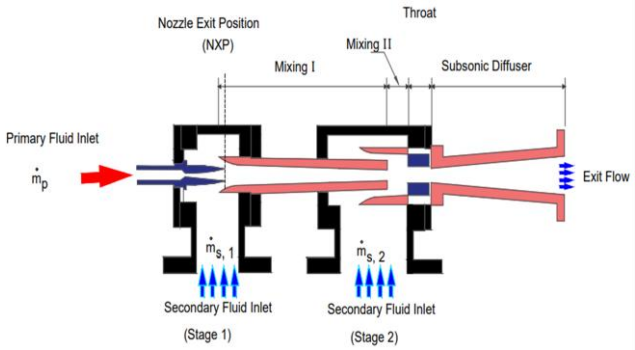

Fig. 1. Schematic of a two-stage ejector.

1.1. Performance evaluation

Performance evaluation of a TSE involves assessing the efficiency and effectiveness of a system that uses two ejectors in series to entrain and compress the secondary fluid (suction fluid). This configuration allows for higher compression ratios and is often used in applications requiring higher pressures, such as in studies involving entrainment ratio, discharge pressure, suction pressure, critical pressure ratio, and experimental testing.

1.2. Entrainment ratio

The entrainment ratio of a two-stage ejector denotes the proportion of mass flow rate attributed to the secondary fluid (often referred to as entrained or suction fluid) with respect to the flow rate of primary fluid (typically termed motive fluid) within each stage of the ejector. The equation which can be used to calculate the entrainment ratio is given as follows:

$$ER = \frac{\dot{m}_{s,1}+\dot{m}_{s,2}}{\dot{m}_p}. \quad (1)$$

Here, $\dot{m}_{s,1}$ is the mass flow rate of the secondary fluid entrained at the first stage, where the primary fluid (motive fluid)

interacts with the secondary fluid. The mixed fluid from the first stage then acts as the motive fluid for the second stage, entraining an additional secondary mass flow rate $\dot{m}_{s2}$ at the second inlet. This distinction ensures that the contributions of both stages to the overall entrainment are clearly captured.

1.3. Compression ratio/lift pressure ratio

The compression ratio is given as follows:

$$CR = \frac{P_{dis}}{P_{suc}}. \quad (2)$$

Here, P_{dis} denotes the pressure at the discharge boundary, and P_{suc} signifies the pressure at the suction boundary.

Although single-stage ejectors are frequently used to create vacuum, they have some disadvantages that can affect their performance in some applications, including limited vacuum generation, decreased efficiency, reduced performance at low pressures, and a larger size. However, the addition of a two-stage ejector contributes to getting over these restrictions as explained by various researchers.

In the study of a two-stage ejector [16], the numerical technique utilising Navier-Stokes equations and the theoretical assessment using a 1-dimensional model have been used to critically evaluate the flow phenomena within ejector systems. Existing experimental data were used to validate both numerical and theoretical results. In [17], to determine the ideal design parameters, numerical studies utilising computational methods were used to estimate the performance phenomena of the two-stage ejector system. It has been suggested that a TSE system is a valuable different configuration for making use of the fired thrust of the discharged flow. As compared to the traditional single-stage ejector system, the performance can be greatly enhanced. It is shown in [18] that the two-stage ejector-diffuser system performs approximately four times better than the single ejector system. A trial exploration of a two-stage ejector refrigeration system, encompassing activities such as design of the system, operation, and empirical assessment was made in [19]. It was examined using independently varying temperatures for evaporation and condensation to examine the likelihood for a system performance change. The blended performances of both the ejectors used in the two-stage ejector-based multi-evaporator refrigeration system (TEMERS) were examined in [20] utilising a two-dimensional CFD modelling method. First, the cooling capacity requirements of the refrigeration and air-conditioning chamber define the main nozzle diameters. Using the verified Reynolds-averaged Navier–Stokes (RANS) simulation model, a shape optimisation was performed to maximise the entrainment performance of the R134a two-phase ejector [21]. The suggested review updates the body of prior research on the topic by talking about the pertinent and latest material. Expressive and latest improvements in refrigeration cycles, two-phase ejector modelling and other potential applications are shown and addressed in their respective contexts [22]. The concept of a two-stage ejector design was proposed, incorporating a second inlet. In the replication, the steam ejector refrigeration system's varied operating parameters were used to evaluate the TSE performance, which was then compared to the SSE performance [23]. The current two-stage ejector, which is CRMC-based, can highlight recent and important developments in the area based on supersonic design. ANSYS Fluent 14.0 was used to examine the calculated model numerically for the specified design input parameters and was validated by numerical data [24]. Using thermodynamic analytical techniques, the two-stage cascade refrigeration cycle (CARC) with an enhanced ejector was compared in [25] with the conventional CARC for effectiveness. It has been suggested that the TSE should replace the single-stage ejector due to its superior geometrical configuration, which allows better utilisation of the discharge flow's terminated momentum to generate secondary flow [26]. To upgrade the energy effectiveness of the refrigeration system on a fishing craft, the study [27] proposed a TSE based subzero refrigeration system in order to construct and achieve the best entrainment performance, where each stage's specified parameter is developed with the consideration of the area ratio. A pattern of established and newly developed exergy approaches is utilised in [28] to assess the exergy destruction properties inside the system. Another investigation provides the optimum design and process control methodologies for the hydrogen passage system with a dual ejector to support all aspects of PEMFC system processes [29]. To enhance CO_2 two-phase ejectors' off-design performance, a new swirl-bypass nozzle ejector-based design is put forth in [30]. A 3D multiphase CFD is used to investigate the design of such a device. This study looks at the impact of adding an ejector to two-phase cascades for refrigeration at very low temperatures. The impacts of various ejector configurations on thermodynamics, the environment, and the economy are compared. The main characteristics examined are the volumetric chilling capacity, best cascade temperature, economic analysis, and total equivalent warming impact (TEWI). The impact of various refrigerants on the cycle of low-temperature of the two-stage cascade is also examined [31]. The report [32] presents the findings of a computer-based fluid dynamic study on the TSE execution in a system of refrigeration using a steam ejector, along with a comparison to an SSE without altering the ejector's area ratio. There is a discussion of the elevated entrainment ratio, coefficient of performance (COP), and the additional adaptable TSE functioning.

Environmentally friendly refrigerants are replacing those whose use is either completely prohibited or highly restricted by the Kyoto Protocol. One such refrigerant, R134a, has had its use restricted and will eventually be completely outlawed. R134a has several substitutes, and various studies have been performed to determine possible replacements based on performance criteria. In the study [33], the effects of using R1234ze€, R1234yf, or R600a as an alternative for R134a in the ejector-based bus air conditioning for single and dual ejectors were investigated. Given the increasing demand for heating, the implementation of high-efficacy heating within combined heat and power systems is regarded as a pragmatic method toward conserving energy and reducing emissions [34]. A novel two-stage ejector featuring a control switching technique is presented in [35]. The main purpose is to ensure consistent and stable performance of the TSE across a wide range of primary flow pressures. To achieve this, an optimal switching approach has been devised. Accord-

ing to the numerical findings, when 60% of the pressure reaches the specified primary flow pressure, the TSE demonstrates an impressive 79.4% increase in entrainment ratio as compared to the traditional single-stage ejector.

Recently, the multi-stage ejector is considered as a high-performance device as compared to a single stage ejector. In the present study, the 1-D gas dynamic model of a single stage ejector is modified by creating a second opening at the exit of the mixing section, where the secondary flow can again be dragged through the momentum of the mixed fluid from a single stage. ANSYS Fluent 18.0 is used to analyse the two-stage ejector geometry for on and off design operating conditions.

2. Mathematical computation of the two-stage ejector geometry

The analysis is limited to the axi-symmetric ejector. This section explains the compressible flow theory in one dimension, utilising the CRMC method with frictional effects for real fluids. The design approach is based on the equations of steady flow in an adiabatic steady-state system.

2.1. Computation of flow properties at the exit from the mixing region for a two-stage ejector.

In addition, SSE [36] was modified to become a TSE. Utilising superfluous momentum from the initial stage to further entrain the secondary flow is made possible by the TSE's additional entrainment passageway at the mixing section's outlet. The geometry calculation procedure for a TSE is nearly identical to that of a single-stage supersonic ejector, except for the calculation of the ejector's second stage. To determine the equilibrium properties at the ejector section J-J', which is necessary for computing the TSE diffuser region, certain alterations were completed to the creation of section J-J', which is shown in Fig. 2. The regions of nozzle and mixing area of the computed two-stage ejector remain the same as those of the single-stage ejector (SSE), but the diffuser section of TSE was computed separately. The geometry of TSE is computed using the CRMC approach with the key parameters including the nozzle diameter (d_n = 99.5 mm), mixing section length (L_m = 95 mm), and diffuser length (L_d = 250 mm), as illustrated in Fig. 3. These parameters are derived from the 1D gas dynamic model to ensure optimal entrainment and pressure recovery.

$$C_{n,e} = C_{m,e}, \tag{3}$$

$$\varphi \rightarrow \varphi = \frac{\dot{m}_{s,2}}{\dot{m}_{m,e}}, \tag{4}$$

$$\dot{m}_{m,e} = \dot{m}_p + \dot{m}_{s1}, \tag{5}$$

$$T_{0,p} \rightarrow T_{o,m}, \tag{6}$$

$$T_{0,s1} \rightarrow T_{o,s2}, \tag{7}$$

$$T_{0,s1} \rightarrow T_{0,s2}, \tag{8}$$

$$\rho_{0,s1} \rightarrow \rho_{0,s2}. \tag{9}$$

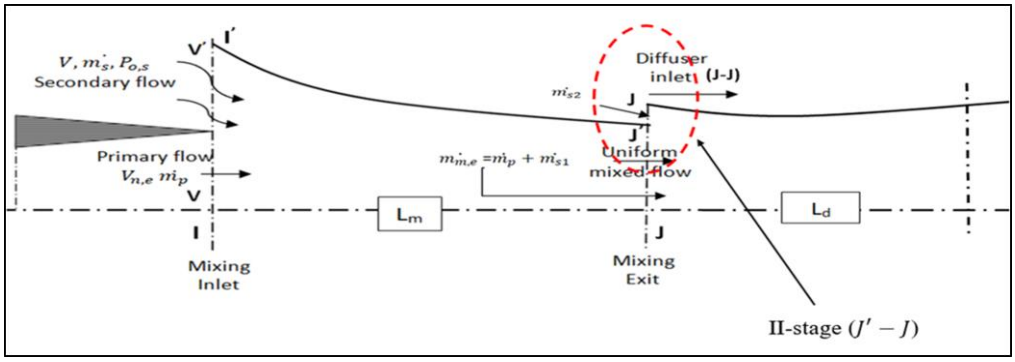

Fig. 2. Discrete modelling of a two-stage ejector.

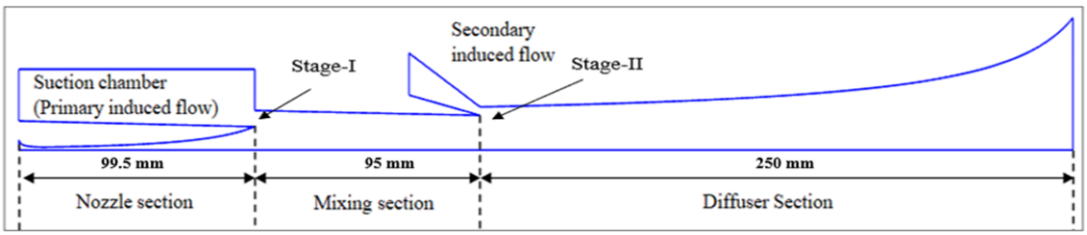

Fig. 3. CRMC two-stage ejector system.

2.3 Selection of design conditions

The working fluid for both primary and secondary flows is water vapour (steam). Steam superheating is critical for ejector performance, as it ensures that the primary flow remains gaseous during expansion in the nozzle, preventing condensation that could disrupt supersonic flow and reduce entrainment efficiency. The degree of superheating, defined as the temperature difference above the saturation point at a given pressure, enhances the thermal energy available for driving the entrainment process. For

the primary flow, a superheating degree is approximately 30 K above the saturation temperature, which ensures stable operation and maximises momentum transfer to the secondary flow.

The primary flow is superheated steam at a pressure of 2.2 bar and temperature of 423 K, with a superheating degree of approximately 30 K above the saturation temperature. The secondary flow is at 0.014 bar and 300 K, as specified in Table 1. To conduct the analytical and numerical examination, the design data points specified in Table 1 were taken into consideration.

Table 1. Design data points for two-stage ejector.

Parameters	Primary flow	Secondary flow
Pressure (Pa)	2.2×105	1×103
Temperature(K)	423	300
Degree of superheating (K)	30	0 (saturated)
Mass flow rate(kg/s)	0.01	–
Nozzle exit position = 0	–	–

3. Computational analysis

The chapter describes the use of a 1-D gas dynamic approach and computational fluid dynamics (CFD) for designing and optimisation of ejector systems. The 1-D gas dynamic approach considers axi-symmetric, steady, turbulent, compressible flow that is equivalent to area-averaged axis-symmetric flow. This approach is used to generate the ejector geometry, which is required for CFD analysis. The ANSYS Fluent 18.0 commercial software is used for CFD analysis, and it is specifically designed for simulating turbulent supersonic flow. This software is efficient in optimising and simulating flow properties, which can help in improving the ejector system's performance. It is important to note that CFD analysis can only be performed when the geometry is known. Therefore, the 1-D gas dynamic CRMC approach is a necessary step in the ejector system design process. The ejector geometries are quantified through a comprehensive study using ANSYS Fluent 18.0. Overall, the combination of the 1-D gas dynamic approach and CFD analysis can provide a powerful tool for designing and optimising ejector systems.

The evaluation of flow properties such as the Mach number, pressure, and temperature has been carried out along ejector's axial direction. The computation of the 'entrainment ratio,' a universal performance parameter, has been supported by the outcomes predicted by the 1-D gas dynamic model under on-design conditions. Additionally, the ejector's off-design features were examined to ascertain its adaptability to varying operating conditions and working fluids in diverse fields of application. In the off-design investigation, parameters were varied one at a time, while the remaining parameters were kept constant.

The Navier-Stokes equation was numerically solved for the 2-dimensional axi-symmetric field using a steady-state turbulence model. Listed below are the governing equations in the compact Cartesian form [36]:

- mass equation:

$$\frac{\partial}{\partial x_i}\left(\rho u_j\right) = 0, \tag{10}$$

- momentum equation:

$$\frac{\partial}{\partial x_i}\left(\rho u_i u_j\right) = -\frac{\partial P}{\partial x_i} + \frac{\partial \tau_{ji}}{\partial x_j}, \tag{11}$$

where:

$$\tau_{ij} = \mu_{eff}\left(\frac{\partial u_i}{\partial x_j} + \frac{\partial u_j}{\partial x_i}\right) - \frac{2}{3}\mu_{eff}\frac{\partial u_k}{\partial x_k}\beta_{ij}, \tag{12}$$

- energy equation:

$$\frac{\partial}{\partial x_i}\left(u_i(\rho E + P)\right) = \vec{\nabla}.\left(\varepsilon_{eff}\frac{\partial T}{\partial x_i} + u_j\tau_{ji}\right). \tag{13}$$

Here, ρ is the mixture density, u is the velocity vector, E – total energy, P – pressure, ε_{eff} – effective thermal conductivity, μ_{eff} – effective dynamic viscosity and β_{ij} is the Kronecker function.

The shear stress transport (SST) k–ω turbulence model was selected for numerical simulation of the supersonic ejector configuration due to its superior ability to capture mixing layers and simulate free shear flows in round and radial jets, which are critical for accurately modelling the complex flow interactions in TSE. Unlike the k–ε model, which is less effective in resolving near-wall effects and separated flows, the k–ω SST model combines the robustness of k–ω near walls with the accuracy of k–ε in free-stream regions, making it ideal for this study (Ariafar et al. [37]). Below are the governing equations of this model:

- turbulence kinetic energy:

$$\frac{\partial}{\partial x_i}(\rho k u_i) = \frac{\partial}{\partial x_j}\left[\left(\mu + \frac{\mu_t}{\sigma_k}\right)\frac{\partial k}{\partial x_j}\right] + G_k - Y_k + S_k, \tag{14}$$

- specific dissipation rate:

$$\frac{\partial}{\partial x_i}(\rho\omega u_i) = \frac{\partial}{\partial x_j}\left[\left(\mu + \frac{\mu_t}{\sigma_\omega}\right)\frac{\partial \omega}{\partial x_j}\right] + G_\omega - Y_\omega + D_\omega + S_\omega. \tag{15}$$

Here:

$$G_k = -\overline{\rho u_i' u_j'}\frac{\partial u_j}{\partial x_i}, \qquad Y_k = \rho\beta^* k\omega, \qquad Y_\omega = \rho\beta\omega^2,$$

$$D_w = 2(1 - F_1)\,\rho\sigma_{\omega,2}\,\frac{1}{\omega}\frac{\partial k}{\partial x_i}\frac{\partial \omega}{\partial x_j},$$

where G_k, Y_k and S_k are the generation of turbulent kinetic energy owing to mean velocity gradients, the generation of turbulence kinetic energy owing to buoyancy and the influence of the variable dilatation in compressible turbulence on the overall dissipation rate, respectively. These terms are expressed as in ANSYS Fluent 18.0 (user manual). G_ω and Y_ω represent generation and dissipation of omega, respectively.

ANSYS Fluent 18.0 was used to employ control volume-based discretisation techniques in solving the governing equations of the problem. The equation's conventional terms were discretised using a second-order upwind approach in order to attain higher-order precision. After that, an implicit method was used to resolve the subsequent arithmetic equations using a density-based joint solver. The algorithm stability was maintained by setting a CFL criterion of 5. At the primary and secondary flow exits and inlets of both ejectors, the pressure boundary condition was applied. In order to achieve greater orthogonality and

better control over mesh quality, the structured quadrilateral mesh was employed in the computational zone of TSE geometries (Fig. 4). There were comparatively more cells used in the area with the higher velocity gradient.

The boundaries are assumed to have zero normal gradients (refer to Fig. 5), resulting in no-slip conditions. In all simulation scenarios, the convergence criterion for the continuity equation and various equations, including *X* and *Y* velocities, energy, turbulence kinetic energy, and turbulence dissipation rate, is set to 10^{-5}. For the TSE geometry, the residual convergence criterion for the continuity equation is 10^{-9}. The supersonic flow computational model is solved using a second-order upwind scheme with an under-relaxation factor of 0.3, and standard wall treatment is used near the wall.

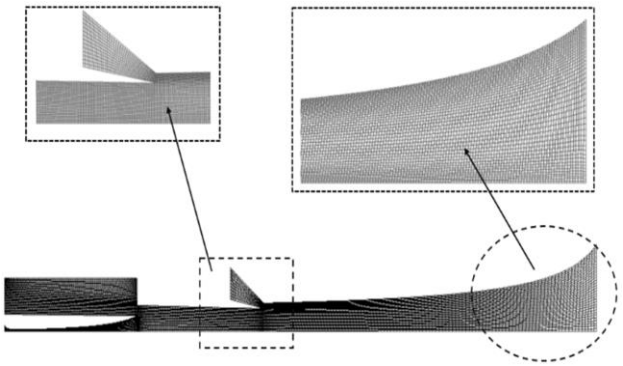

Fig. 4. CRMC two-stage ejector computational domain.

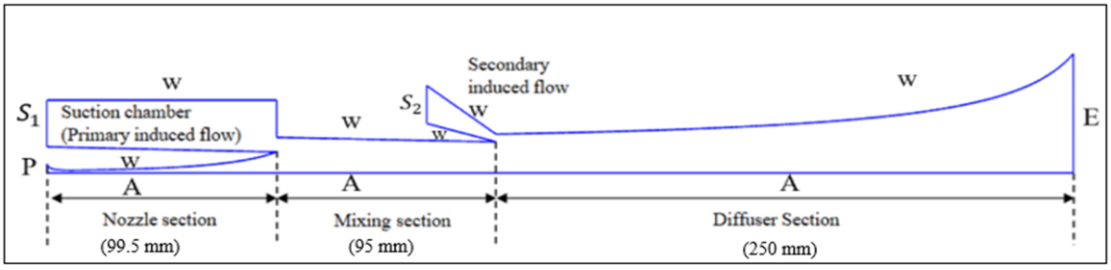

Fig. 5. Boundary conditions employed in TSE ejector computational domain.

3.1. Grid Independence study

The k–ω SST model was used to conduct a grid independence study on both computational domains. Initially, 60 432 elements were created. The grid-independence study was conducted to assess the performance parameter known as the "entrainment ratio". This study involved increasing the number of grid elements from 60 432 to 110 246. The results indicated that the variation was less than 5%. Based on this assessment, the number of elements was established at 110 246. However, a higher number of grid elements was defined in the ejector's mixing region to accurately capture the mixing phenomenon. The mesh quality was assessed based on the mesh orthogonality and aspect ratio. The results (refer to Table 2) indicate that changes of the entrainment ratio were insignificant beyond ~110 246 elements, thus further study was conducted using the number of cells around this value.

Table 2. Detailed mesh used for TSE computational domain.

Model No.	No. of cell	Entrainment ratio (φ)
TM-1	60432	0.624
TM-2	80642	0.649
TM-3	**110246**	**0.657**
TM-4	130324	0.658
TM-5	150132	0.656

4. Validation of the CRMC approach for the two-stage ejector diffuser section

The validation of the 1D ejector model incorporating the CRMC approach with CFD was carried out. The purpose of this validation was to verify the 1D ejector model before advancing to the study of operating parameters. On-design data (see Table 1) were used for this analysis. The results obtained from the CFD study, particularly the static pressure, were compared with those calculated from the 1D ejector model under design conditions. In the CFD results, the combined flow of the single-stage ejector and the secondary auxiliary fluid enters and mixes at the second stage, exhibiting oscillations near the diffuser inlet. However, this behaviour is not captured by the 1D ejector model. The static pressure variation along the diffuser region of the 1D ejector model and CFD centreline results are shown in Fig. 6. Mixed fluid of SSE and secondary auxiliary fluid exchange their kinetic energy and momentum during mixing and grasp up to equilibrium with uniform flow properties. The flow downstream of the diffuser shows a diminishing deviation.

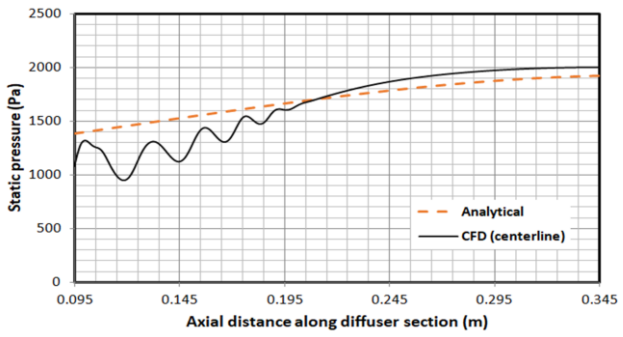

Fig. 6. Variation of static pressure along the diffuser section under on-design conditions (P_{osp} = 2.2 bar, P_{oss}=0.014 bar, P_e= 0.01925 bar).

5. Results and discussion

The computational study has been performed on the two-stage ejector model, which was considered for mathematical study. The effect of operating parameters on the performance of the ejector model is presented here. Mach number contours are employed to analyse the operating effects on the performance.

Figure 7 shows the contours of Mach number. The flow characteristics within the ejector can be perceived along with first and second series of oblique shock waves, diamond wave and shear layer. The primary supersonic flow and secondary subsonic flow start interacting after entering the mixing section, and move towards the second stage with uniform flow properties. The effective area plays an important role for entering secondary flow. The uniformly mixed fluid from SSE acts as the primary fluid, enabling further entrainment of secondary fluid in TSE.

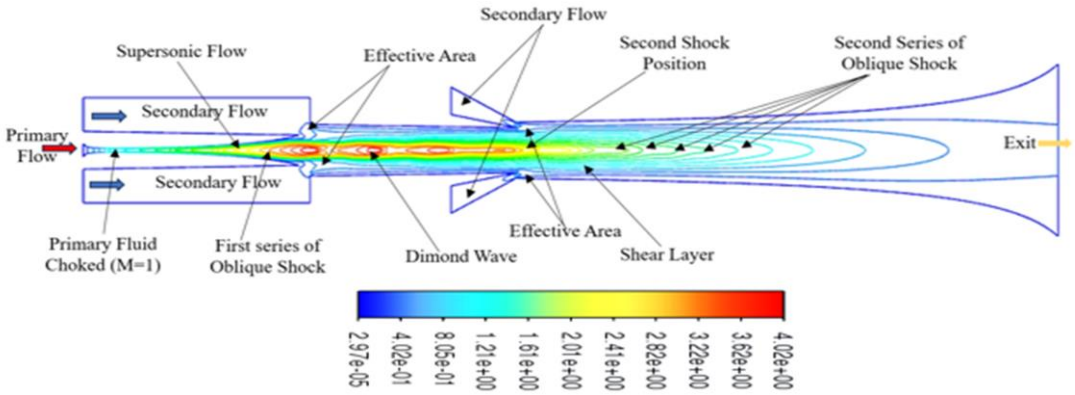

Fig. 7. Mach number contours of the two-stage ejector under on-design conditions ($P_{o,p}$ = 2.2 bar, $P_{o,s}$=0.014 bar, P_e= 0.01925 bar).

5.1. On-design study

A CFD examination was conducted to analyse the design of two-stage ejectors. Figure 8 displays the pressure fluctuations during the regions of mixing and diffuser. At stage I, the primary and secondary fluid flows strongly interact, causing pressure pulsation in the mixing section. Furthermore, pressure oscillation was noted in the diffuser section as a result of the contact of secondary and mixed flow at stage II.

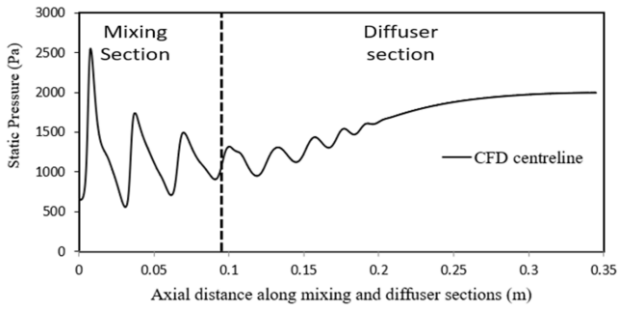

Fig. 8. Static pressure variation along the two-stage ejector under on-design conditions ($P_{o,p}$ = 2.2 bar, $P_{o,s}$=0.014 bar, P_e= 0.01925 bar).

The pressure gradually increased in the diffuser region after the mixing of the motive and secondary fluids at both stages. The static pressure at the diffuser section exit was predicted to be 0.01925 bar through numerical analysis.

Figure 9 depicts the Mach number fluctuation throughout the two-stage ejector. The anticipated Mach number at the centreline calculated numerically is 4.3, while the design Mach number determined analytically is 3.03. The average Mach number was taken from the analytical design, whereas the centreline Mach number was obtained from the CFD investigation.

Figure 10 displays the overall pressure fluctuation occurring alongside the mixing and diffuser region of TSE. The mixing section exhibits a discernible loss of total pressure (as depicted in Fig. 10) owing to the strong interaction between primary and

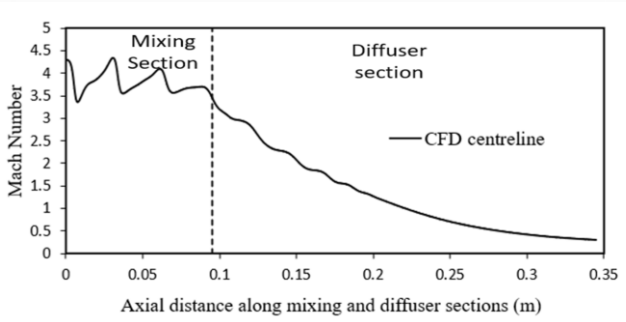

Fig. 9. Mach number variation along the two-stage ejector under on-design conditions ($P_{o,p}$ = 2.2 bar, $P_{o,s}$=0.014 bar, P_e= 0.01925 bar).

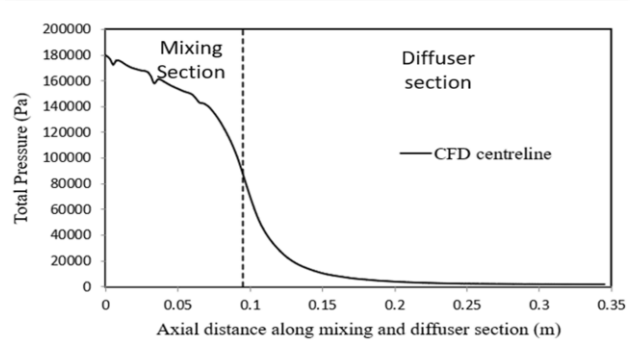

Fig. 10. Total pressure variation along the two-stage ejector under on-design conditions ($P_{o,p}$ = 2.2 bar, $P_{o,s}$=0.014 bar, P_e= 0.01925 bar).

secondary fluid at the section inlet. The shift in the total pressure occurs gradually and uniformly, thanks to the CRMC method that prevents any thermodynamic shock occurring at the diffuser section inlet, unlike for the conventional ejector system.

Figure 11 illustrates the changes in static temperature as it traverses the mixing and diffuser sections of a two-stage ejector system. The static temperature experiences a decrease initially in stage I because of the interplay between the primary and secondary fluid flows. However, it subsequently gradually increases along the diffuser section and ultimately reaches 358 K at the exit of the diffuser section.

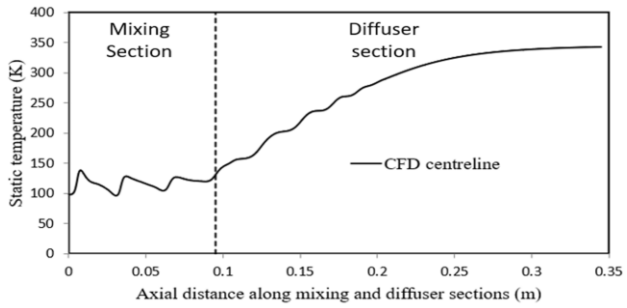

Fig. 11. Static temperature variation along the two-stage ejector under on-design conditions ($P_{o,p}$ = 2.2 bar, $P_{o,s}$=0.014 bar, P_e= 0.01925 bar).

5.2. Off-design optimisation

Numerical analysis has been conducted to examine the performance of the TSE at different operating pressures. One operating pressure was altered at a time while the other remained constant as per the design. The numerical analysis optimised the TSE performance by evaluating the entrainment ratio (φ) under varying primary flow pressure, exit pressure, and nozzle exit position (NXP). The results (Fig. 12) show that the entrainment ratio peaks at a primary flow pressure of 2.2 bar under on-design conditions.

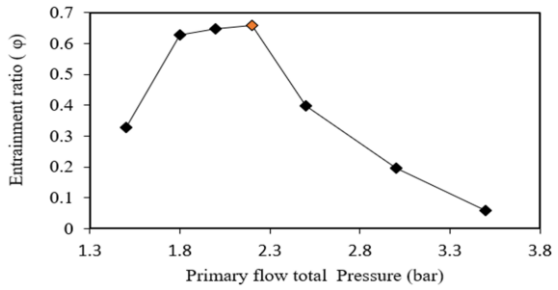

Fig. 12. Effect of entrainment ratio (φ) on primary flow total pressure.

Figure 12 depicts the correlation between the entrainment ratio and the total pressure of the primary flow. The mass inflow and momentum during the nozzle's flow at exit increase when the primary flow's total pressure is raised. In the area of the mixing section, this increase in momentum speeds up the entrainment process. Nevertheless, the secondary mass flow rate that must be entrained in Stages I and II increases more slowly than the primary mass flow rate. Consequently, the entrainment ratio shows an initial rise in stages I and II as the primary flow total pressure increases (below the on-design primary flow total pressure of approximately 2.2 bar). After this point, the entrainment ratio begins to decrease.

Figure 13 displays the Mach number contours of a two-stage ejector, which can help explain the physical phenomena related to this pattern. When the primary flow total pressure increases, the secondary shock location moves downstream, causing the pressure within the suction section to increase for the same exit pressure (P_e = 0.01925 bar). However, above the on-design point, an increase in primary flow pressure decreases the pressure difference inside the suction chamber, reducing the trend to entrain secondary flow. Moreover, due to a decrease in the effective area at stages I and II, the ejector can operate at higher critical pressure levels. Consequently, the overall entrainment ratio decreases.

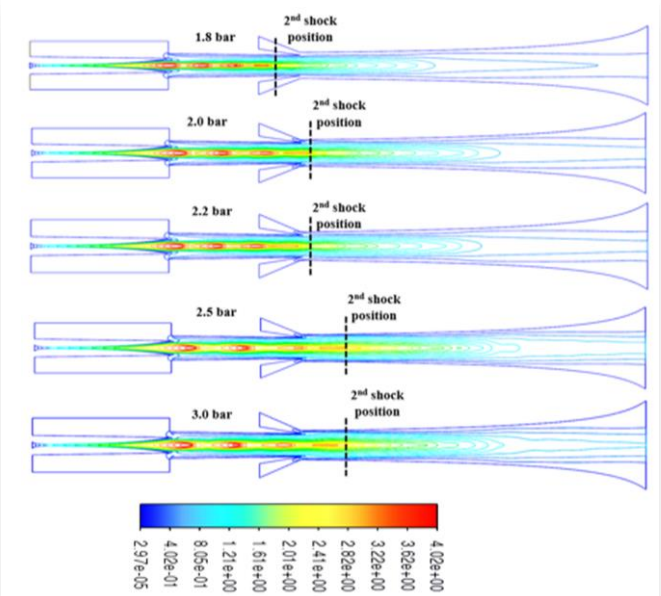

Fig. 13. Primary flow pressure impact on secondary shock position.

Figure 14 depicts how the entrainment ratio changes with the exit pressure. This numerical investigation was conducted when NXP was equal to zero. The ejector's performance curvature is classified into three types: choked, unchoked and reverse flow. As the exit pressure rises, the oblique shock becomes more powerful, and shock waves travel upstream. As a result, both of the flows, i.e. primary and secondary flows, are disrupted at stages I and II.

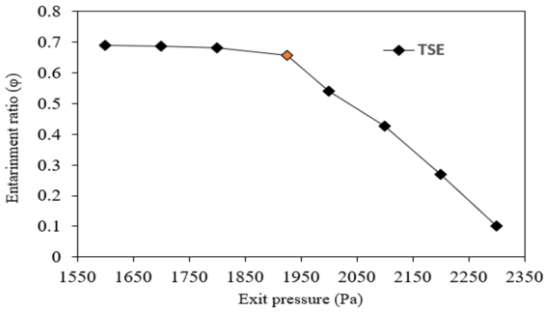

Fig. 14 Effect of exit pressure on entrainment ratio (φ).

When the exit pressure is further increased, the shock waves become stronger and impede the secondary flow from entraining at stages I and II, leading to a reduction in the entrainment ratio.

In this investigation, the ejector was found to operate under double fluid choking at pressures up to 0.01925 bar, with minimal variation in the entrainment ratio. However, when the primary fluid alone was choked (between 0.01925 bar and 0.02300 bar), there was a dramatic decrease in the system's entrainment ratio. The system reached its breakdown point at 0.02350 bar.

To avoid choking of both primary and secondary flows during reverse flow, the primary flow is directed into the suction chamber. This study shows that the ejector must operate in a choked flow region, with a critical pressure separation, to achieve the highest entrainment ratio.

The Mach number contours in Fig. 15 illustrate how the shock position of TSE is influenced by the exit pressure. The second series oblique shock wave position's distance decreases with the increasing exit pressure, which affects the mixing phenomenon in the stage I and II entrainment zone. Still, the entrainment ratio stays constant up to the on-design departure pressure (P_e = 0.01925 bar). Beyond this threshold, the entrainment ratio decreases as exit pressure rises. This study, which relies solely on the CRMC theory, identified the critical exit pressure as the on-design condition for the two-stage ejector through analytical analysis. Numerical analysis confirms that the ejector performs optimally under double choked conditions (primary and secondary flow) at the on-design exit pressure.

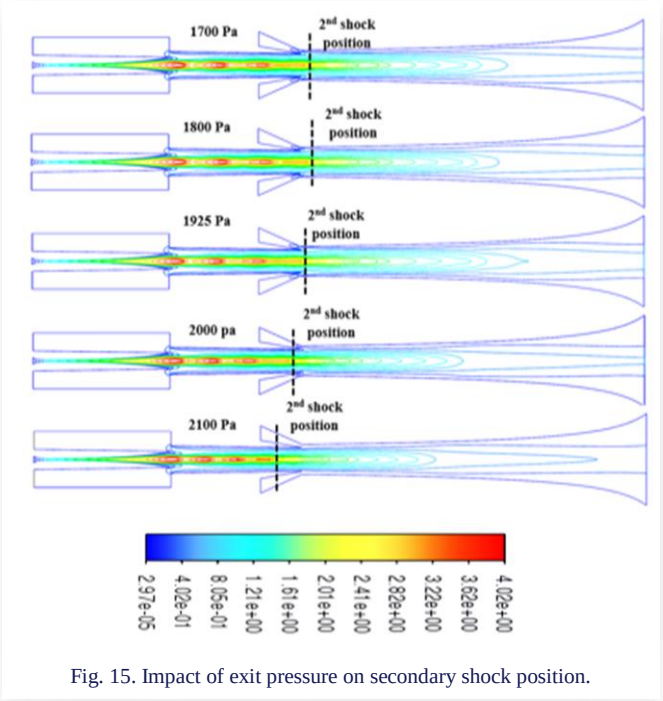

Fig. 15. Impact of exit pressure on secondary shock position.

The placement of the nozzle exit is a critical geometric factor for two-stage ejectors as it dictates the expansion angles of the jet and the converging passageway that induces flow in the entrainment region. In the two-stage ejector system, the entrainment area is not explicitly calculated through analytical modelling. To assess the impact of the nozzle exit position, the variation was tested comparative to the on-design situation (NXP = 0) in both the upstream (−4 mm) and downstream (+3 mm) directions of the flow at 1 mm intervals (refer to Fig. 16). The numerical results demonstrate that the entrainment ratio increases up to −2 mm when moving away from NXP = 0 in the upstream direction, followed by a decrease. Conversely, moving from NXP = 0 into the mixing area when going downstream decreases the entrainment. As a whole, it is clear that adjusting the nozzle exit location away or towards the mixing area from NXP=0 results in a significant alteration of the entrainment ratio.

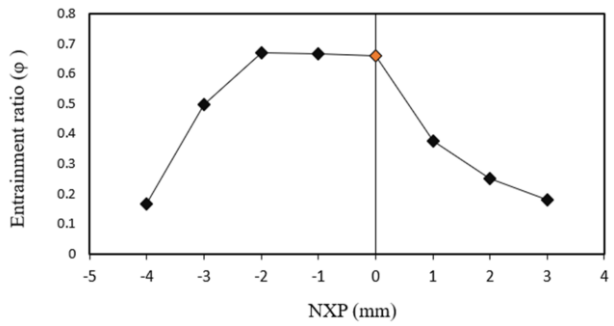

Fig. 16. Effect of entrainment ratio (φ) on nozzle exit position (NXP).

By altering the expansion of the jet and induced flow pathways, entrainment varies with NXP. In the mixing portion, moving downstream lowers the induced flow passage and expansion angle, which lessens entrainment. Furthermore, the momentum of motive flow responsible for induced secondary flow decreases with the increasing distance from the suction port because of positive NXPs. On the other hand, ejector entrainment performance is enhanced when positioned upstream (up to –2 mm from the mixing plane inlet), which increases the expansion angle and induced flow passage. The findings of the CFD and 1-D analyses are compared in Fig. 17.

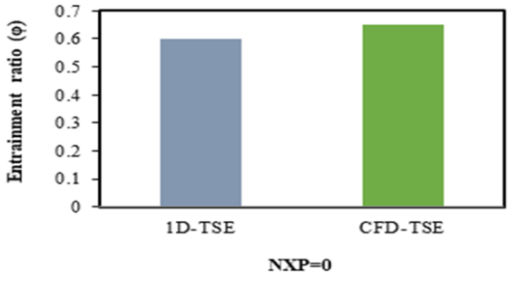

Fig. 17. Comparison of 1-D and CFD entrainment ratios (on-design).

6. Conclusions

The physics based two-stage ejector was designed and validated using on-design CFD results. Operational characteristics like the main fluid pressure, exit fluid back pressure, and nozzle exit location were also subjected to numerical analysis. It has been examined how operating parameters affect the entrainment ratio. The following is a list of the study's findings:

- The flow characteristic inside the two-stage ejector plays a very important role in identifying the oblique shock positions, diamond type wave, effective area and shear layer, and in developing a high performance ejector.
- Mach number contours are taken into consideration in order to forecast the entrainment effect and the flow behaviour inside the ejector.
- The CFD results of static pressure variation closely match the 1D on design ejector obtained results.
- The entrainment ratio increases with the increase in primary pressure up to the on-design pressure. Beyond this value, the entrainment ratio starts to fall if the exit pressure increases.

References

[1] Ma, X., Sun, W., Ma, S., Zhang, H., Zhang, Y., Liu, C., Jia, L., & Xue, H. (2023). A streamlining method for ejector nozzle profile optimization based on polynomial function. *Applied Thermal Engineering*, 219, A, 119380. doi: 10.1016/j.applthermaleng.2022.119380

[2] Muzaber, A., Bassmaji, N., & Kaddah, A. (2024). A new mixing chamber geometry design for supersonic ejector performance optimization using computational fluid dynamics. *International Journal of Thermofluids*, 101047. doi: 10.1016/j.ijft.2024.101047

[3] Zheng, L., Wang, W., Zhang, Y., Wang, L., & Lu, W. (2022). Optimization Analysis of the Mixing Chamber and Diffuser of Ejector Based on Fano Flow Model. *Computer Modelling in Engineering & Sciences*, 133(1), 153–170. doi: 10.32604/cmes.2022.021235.

[4] Yan, J., Li, Z., & Zhang, H. (2023). Investigation on key geometries optimization and effect of variable operating conditions of a transcritical R744 two-phase ejector. *Applied Thermal Engineering*, 230, 120733. doi: 10.1016/j.applthermaleng.2023.120733

[5] Kumar, V., Singhal, G., & Subbarao, P.M.V. (2013). Study of supersonic flow in a constant rate of momentum change (CRMC) ejector with frictional effects. *Applied Thermal Engineering*, 60(1−2), 61−71. doi: 10.1016/j.applthermaleng.2013.06.045

[6] Seth, B., Knecht, S., Szalai, M., & Haußmann, J. (2025). Design of a variable passive ejector for hydrogen recirculation of a PEM fuel cell system. *International Journal of Hydrogen Energy*, 99, 956−965. doi: 10.1016/j.ijhydene.2024.12.091

[7] Khennich, M., Galanis, N., Sorin, M., Orfi, J., Sarrafi, A., & Dupuis, S. (2024). Thermodynamic analysis of a solar powered ejector cooling system. *International Journal of Thermofluids*, 24, 100960. doi: 10.1016/j.ijft.2024.100960

[8] Kanbur, B.B., Kriezi, E.E., Markussen, W.B., Kærn, M.R., Busch, A., & Kristófersson, J. (2025). Framework for prediction of two-phase R-744 ejector performance based on integration of thermodynamic models with multiphase mixture CFD simulations. *Applied Thermal Engineering*, 258, C, 124888. doi: 10.1016/j.applthermaleng.2024.124888

[9] Ogaili, H.H., Khalilarya, S., Chitsaz, A., & Mojaver, P. (2025). Energy, exergy, and economic performance analysis of integrated parabolic trough collector with organic Rankine cycle and ejector refrigeration cycle. *Energy Conversion and Management: X*, 25, 100843. doi: 10.1016/j.ecmx.2024.100843

[10] Fabris, F., Bodys, J., Marinetti, S., Minetto, S., Smołka, J., & Rossetti, A. (2024). Numerical modelling of a single-compression multi-temperature ejector-supported R744 refrigeration unit for last mile delivery. *International Journal of Refrigeration*, 160, 65−75. doi: 10.1016/j.ijrefrig.2024.01.014

[11] Gagan, J., Śmierciew, K., Pawluczuk, A., Łukaszuk, M., Dudar, A., & Butrymowicz, D. (2025). The First experimental tests of novel bivalent hybrid ejector-compressor refrigeration system. *Energy*, 317, 134646. doi: 10.1016/j.energy.2025.134646

[12] Fingas, R., Haida, M., Smolka, J., Croci, L., Bodys, J., Palacz, M., & Besagni, G. (2025). Experimental analysis of the R290 variable geometry ejector with a spindle. *Applied Thermal Engineering*, 258, C, 124632. doi: 10.1016/j.applthermaleng.2024.124632

[13] Paul, S., Srikar Reddy, P., Rao, S.M., & Kumar, P. (2025). Surrogate model based multi-objective optimisation of supercritical CO_2 ejectors. *The Journal of Supercritical Fluids*, 218, 106493. doi: 10.1016/j.supflu.2024.106493

[14] Siddique, S.M., Uzzaman, M.M., Ehsan, M.M., & Khan, Y. (2025). Thermal analysis of a novel configuration of double effect absorption system cascaded with ejector and injection enhanced compression refrigeration cycle. *Energy Conversion and Management*, 326, 119435. doi: 10.1016/j.enconman.2024.119435

[15] Li, M., Xu, L., & Gong, H. (2025). Examination of an Ejector-Enhanced Geothermal Plant for Power Generation Improvement. *Renewable Energy*, 242, 122400. doi: 10.1016/j.renene.2025.122400

[16] Kong, F., & Kim, H.D. (2015). Analytical and computational studies on the performance of a two-stage ejector–diffuser system. *International Journal of Heat and Mass Transfer*, 85, 71−87. doi: 10.1016/j.ijheatmasstransfer.2015.01.117

[17] Ding, Z., Wang, L., Zhao, H., Zhang, H., & Wang, C. (2016). Numerical study and design of a two-stage ejector for subzero refrigeration. *Applied Thermal Engineering*, 108, 436−448. doi: 10.1016/j.applthermaleng.2016.07.104

[18] Kong, F., & Kim, H.D. (2016). Optimization study of a two-stage ejector–diffuser system. *International Journal of Heat and Mass Transfer*, 101, 1151−1162. doi: 10.1016/j.ijheatmasstransfer.2016.05.129

[19] Chen, G., Zhang, R., Zhu, D., Chen, S., Fang, L., & Hao, X. (2017). Experimental study on two-stage ejector refrigeration system driven by two heat sources. *International Journal of Refrigeration*, 74, 295−303. doi: 10.1016/j.ijrefrig.2016.10.010

[20] Yan, J., Wen, N., Wang, L., Li, X., Liu, Z., & Li, S. (2018). Optimization on ejector key geometries of a two-stage ejector-based multi-evaporator refrigeration system. *Energy Conversion and Management*, 175, 142−150. doi: 10.1016/j.enconman.2018.08.110

[21] Baek, S., & Song, S. (2018). Numerical study for the design optimization of a two-phase ejector with R134a refrigerant. *Journal of Mechanical Science and Technology*, 32, 4231−4236.

[22] Aidoun, Z., Ameur, K., Falsafioon, M., & Badache, M. (2019). Current advances in ejector modeling, experimentation and applications for refrigeration and heat pumps. Part 2: Two-phase ejectors. *Inventions*, 4(1), 16. doi: 10.3390/inventions4010016

[23] Suvarnakuta, N., Pianthong, K., Sriveerakul, T., & Seehanam, W. (2020). Performance analysis of a two-stage ejector in an ejector refrigeration system using computational fluid dynamics. *Engineering Applications of Computational Fluid Mechanics*, 14(1), 669−682. doi: 10.1080/19942060.2020.1756913

[24] Yadav, S.K., Pandey, K.M., Kumar, V., & Gupta, R. (2021). Computational analysis of a supersonic two-stage ejector. *Materials Today: Proceedings*, 38, 2700−2705. doi: 10.1016/j.matpr.2020.08.483

[25] Bai, T., Lu, Y., Yan, G., & Yu, J. (2021). Performance analysis of an ejector enhanced two-stage auto-cascade refrigeration cycle

for low temperature freezer. *Journal of Thermal Science*, 30, 2015−2026. doi: 10.1007/s11630-020-1290-6

[26] Kumar, A., Kumar, V., Subbarao, P.M.V., Yadav, S.K., & Singhal, G. (2022). Numerical assessment on the performance of variable area single-and two-stage ejectors: A comparative study. *Proceedings of the Institution of Mechanical Engineers, Part E: Journal of Process Mechanical Engineering*, 236, 1, 114−125. doi: 10.1177/09544089211033129

[27] Wang, X., Wang, L., Song, Y., Deng, J., & Zhan, Y. (2021). Optimal design of two-stage ejector for subzero refrigeration system on fishing vessel. *Applied Thermal Engineering*, 187, 116565. doi: 10.1016/j.applthermaleng.2021.116565

[28] Yang, D., Li, Y., Xie, J., & Wang, J. (2022). Exergy destruction characteristics of a transcritical carbon dioxide two-stage compression/ejector refrigeration system for low-temperature cold storage. *Energy Reports*, 8, 8546−8562. doi: 10.1016/j.egyr.2022.06.066

[29] Chen, L., Xu, K., Yang, Z., Yan, Z., & Dong, Z. (2022). Optimal design and operation of dual-ejector PEMFC hydrogen supply and circulation system. *Energies*, 15(15), 5427. doi: 10.3390/en15155427

[30] Ringstad, K.E., Banasiak, K., Ervik, Å., & Hafner, A. (2022). Swirl-Bypass Nozzle for CO2 Two-Phase Ejectors: Numerical Design Exploration. *Energies*, 15(18), 6765. doi: 10.3390/en15186765

[31] Udroiu, C.M., Mota-Babiloni, A., Giménez-Prades, P., Barragán-Cervera, Á., & Navarro-Esbrí, J. (2023). Two-stage cascade configurations based on ejectors for ultra-low temperature refrigeration with natural refrigerants. *International Journal of Thermofluids*, 17, 100287. doi: 10.1016/j.ijft.2023.100287

[32] Suvarnakuta, N., Pianthong, K., Sriveerakul, T., & Seehanam, W. (2020). Performance analysis of a two-stage ejector in an ejector refrigeration system using computational fluid dynamics. *Engineering Applications of Computational Fluid Mechanics*, 14(1), 669−682. doi: 10.1080/19942060.2020.1756913

[33] Ünal, Ş., Erdinç, M.T., Akgün, H., & Bilgili, M. (2023). Effects of alternative refrigerants on the ejector dimensions for single and dual ejectors enhanced bus air conditioning system. *International Communications in Heat and Mass Transfer*, 143, 106685. doi: 10.1016/j.icheatmasstransfer.2023.106685

[34] Pang, J., Ge, Z., Zhang, Y., & Du, X. (2023). Comparative designs and optimizations of the steam ejector for a CHP system. *Applied Thermal Engineering*, 226, 120345. doi: 10.1016/j.applthermaleng.2023.120345

[35] Han, Q., Liu, C., Xue, H., Zhang, H., Sun, W., Sun, W., & Jiaa, L. (2023). Working condition expansion and performance optimization of two-stage ejector based on optimal switching strategy. *Energy*, 282, 128376. doi: 10.1016/j.energy.2023.128376

[36] Yadav, S.K., Pandey, K.M., Gupta, R., & Kumar, V. (2021). Numerical study for the influences of nozzle exit position, mixing, and diffuser section lengths on performance of CRMC ejector. *Journal of the Brazilian Society of Mechanical Sciences and Engineering*, 43(496), 1−14. doi: 10.1007/s40430-021-03207-x

[37] Ariafar, K., Buttsworth, D., Al-Doori, G., & Malpress, R. (2015) Effect of mixing on the performance of wet steam ejectors. *Energy*, 93, 2030–2041. doi: 10.1016/j.energy.2015.10.082